THE JOURNAL OF PHYSICAL CHEMISTRY A

Article

pubs.acs.org/JPCA

Insights from Arsenate Adsorption on Rutile (110): Grazing-Incidence X-ray Absorption Fine Structure Spectroscopy and DFT+U Study

Li Yan,[†] Shan Hu,[†] Jinming Duan,[‡] and Chuanyong Jing*,[†]

[†]State Key Laboratory of Environmental Chemistry and Ecotoxicology, Research Center for Eco−Environmental Sciences, Chinese Academy of Sciences, P.O. Box 2871, Beijing 100085, China

[‡]School of Environmental and Municipal Engineering, Xi'an University of Architecture and Technology, Xi'an 710055, China

Supporting Information

ABSTRACT: Insights into the bonding of As(V) at the metal oxide/aqueous interface can further our understanding of its fate and transport in the environment. The motivation of this work is to explore the interfacial configuration of As(V) on single crystal rutile (110) using grazing-incidence X-ray absorption fine structure spectroscopy (GI-XAFS) and planewave density functional calculations with on-site repulsion (DFT+U). In contrast to the commonly considered corner-sharing bidentate binuclear structure, tetrahedral As(V) binds as an edge/corner-sharing tridentate binuclear complex on rutile (110), as evidenced by observation of three As−Ti distances at 2.83, 3.36, and 4.05 Å. In agreement with the GI-XAFS analysis, our DFT+U calculations for this configuration resulted in the lowest adsorption energy among five possible alternatives. In addition, the electron density difference further demonstrated the transfer of charge between surface Ti atoms and O atoms in AsO_4. This charge transfer consequently induced the formation of a chemical bond, which is also confirmed by the partial density of states analysis. Our results may shed new light on coupling the GI-XAFS and DFT approaches to explore molecular-scale adsorption mechanisms on single crystal surfaces.

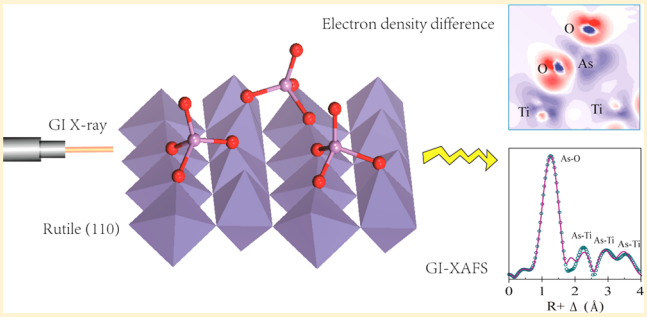

1. INTRODUCTION

The interaction of As(V) with metal (hydr)oxides plays an important role in its distribution and mobility in aquatic systems. As a model metal oxide, titanium dioxide has been successfully used in As(V) removal due to its high adsorption affinity and chemical stability.[1] Our previous X-ray absorption fine structure (XAFS) spectroscopy studies using TiO_2 powders demonstrated the formation of bidentate binuclear As(V) surface complexes.[2,3] However, one intrinsic difficulty with this powder-sample approach is the lack of surface-specific information, because such an XAFS signal is a weighted summation with contributions from different crystal surfaces.[4] Thus, the configuration of surface complexes on a single crystal TiO_2 surface is poorly constrained.

To explore adsorption configurations on crystallographically anisotropic single crystal surfaces, grazing-incidence XAFS (GI-XAFS) has been successfully used in several studies.[4−7] For example, Waychunas et al. studied As(V) surface complexation on hematite (0001) and (10−12) surfaces using GI-XAFS,[6] and the results indicate that edge-sharing bidentate complexes are predominant, in contrast to corner-sharing complexes as evidenced by XAFS analysis on powdered hematite.[8] The discrepancies between GI-XAFS and powder-XAFS results motivated our study, because the unique information acquired by GI-XAFS on single crystal surfaces could not be obtained with conventional XAFS on powdered samples.

In addition to spectroscopic methods, density function theory (DFT) calculations have been used to interpret the adsorption mechanism of As(V) on metal (hydr)oxides.[9−11] DFT studies on As(V)-TiO_2 clusters show that bidentate binuclear and monodentate mononuclear As(V) surface complexes may both exist on the TiO_2 surface.[11,12] However, to the best of our knowledge, study investigating the adsorption mechanism of As(V) on single crystal TiO_2 using GI-XAFS and DFT calculations has been limited. Nevertheless, this missing molecular-scale knowledge may limit our fundamental understanding of As(V) reactions at specific sites on single crystal TiO_2 surfaces.

The objective of this study is to explore the atomic interfacial configurations of As(V) on the rutile (110) surface using GI-XAFS and DFT calculations. Our results suggest that an edge/corner-sharing tridentate adsorption complex dominates the chemisorption of As(V) on the rutile (110) surface. The insight gained from this study sheds new light on combining experimental and computational methods to obtain molecular-level information on surface complex structures.

Received: January 5, 2014
Revised: June 11, 2014
Published: June 12, 2014

2. EXPERIMENTAL AND THEORETICAL METHODS

Materials. Single crystal rutile (110) was purchased from Hefei Kejing Materials Technology Co., LTD (China) and used without further treatment. The As(V) stock solution of 150 mg/L was prepared by dissolving $Na_2HAsO_4{\cdot}7H_2O$ (Fisher Scientific, USA) in 0.04 M $NaClO_4$ solution. 0.01 M NaOH and 0.01 M HCl solutions were used to adjust pH. Milli-Q water was used to prepare solutions, with N_2 purging to remove CO_2 at ambient temperature.

GI-XAFS Study. The As K-edge GI-XAFS experiments were performed on beamline BL14W1 at the Shanghai Synchrotron Radiation Laboratory (SSRF), China. A homemade sample holder was designed especially for the GI-XAFS analysis as shown in Figure S1 in Supporting Information (SI). The sample was prepared by equilibrating the rutile (110) crystal in As(V) solution at pH 5.0 for 2 h. To keep the surface from drying, the sample holder was purged with moisture-saturated N_2 gas during the data collection. Data collection was performed in a horizontal sample orientation. The incidence angle of X-rays on the crystal surface was set to 0.15°, which is below the critical angle of rutile (0.198°). Spectra were collected in fluorescence mode using a 4-element silicon drift detector (SDD). An average of three scans was collected to achieve an adequate signal/noise ratio.

The GI-XAFS spectra were analyzed using the Athena and Artemis programs in IFEFFIT.[13] The data processing and fitting approach was similar to that used in our previous study.[3] In addition to As−O and As−Ti single scattering paths (SS), a multiple scattering (MS) triply degenerate As−O−O path was considered.[14] The coordination number (CN) of the first As−O path was set to four. A single ΔE was applied to all shells and varied during the fitting. The theoretical phase shift and amplitude functions were calculated with the ab initio computer code FEFF6 using DFT-optimized atomic clusters. The goodness-of-fit parameters were also calculated and compared including χ^2 and R-factor, the relative error of the fit and data. Good fits occur for $R < 0.02$.

DFT Calculations. DFT calculations were performed with periodic boundary conditions using the Castep package in Materials Studio (Accelrys, San Diego, CA).[15] A planewave cutoff energy of 340 eV was selected during the calculations.[16] Ultrasoft pseudopotentials were used in the treatment of core electrons.[17] The generalized gradient approximation (GGA) approach of Perdew−Burke−Ernzerhof (PBE) was employed to calculate the exchange-correlation energy.[18] To improve the model accuracy in band gap estimation of TiO_2, an on-site Coulomb potential (DFT+U) correction was applied to the 3d electron of Ti atoms.[19−22] $U = 3.0$ eV was chosen in this study in accordance with previous reports of water adsorption on TiO_2.[21,22] A Monhorst-Pack scheme with a $2 \times 1 \times 1$ k-point grid was employed to sample points over the Brillouin zone.[17] The SCF and energy tolerances of 1.0×10^{-6} and 1.0×10^{-5} eV/atom, respectively, were set as the convergence criteria.

Model Building. The bulk unit cell of rutile was first geometry-optimized, resulting in lattice parameters $a = b = 4.594$ Å and $c = 2.959$ Å, which were comparable with the experimental data ($a = b = 4.5922$ Å and $c = 2.9590$ Å, ICSD #24780). The highly accurate results validated the applicability of Castep code to calculate our molecular structures. The rutile (110) surface was cleaved from the optimized bulk structure, eight layers of atoms were extracted, and then a 2×2 supercell was built.[16] A vacuum slab of 15 Å was added to separate each slab in the direction along the surface normal.[17] The top four layers of atoms were relaxed, while the remaining four layers were frozen during the optimization to keep the computational cost relatively low. After tetrahedral AsO_4 was geometrically optimized in a periodic box of 10 Å side-lengths, it was added to the optimized rutile (110) surface to build the initial interfacial structure. To investigate the effect of water on As(V) adsorption, four water molecules were also added around AsO_4. Several mono-, bi-, and tridentate surface complexes were subsequently structure-optimized.

The adsorption energy E_{ads} in eV for each As(V)-rutile surface complex was calculated according to the following equation:[17,18]

$$E_{ads} = E_{As+surf} - (E_{surf} + E_{As})$$

where $E_{As+surf}$ is the total energy of the surface complexes, and E_{surf} and E_{As} represent the energy of rutile (110) surface and As(V), respectively.

To investigate the change of electron density upon adsorption, the electron density difference ($\Delta\rho$) was calculated by subtracting the electron density of the isolated AsO_4 ($\Delta\rho_{As}$) and surface ($\Delta\rho_{surf}$) from the total electron density of the system ($\Delta\rho_{As+surf}$) as follows:[17] $\Delta\rho = \Delta\rho_{As+surf} - (\Delta\rho_{surf} + \Delta\rho_{As})$.

3. RESULTS AND DISCUSSION

Rutile (110) Surface and Possible Adsorption Structures. The features of the rutile (110) surface and the corresponding surface complexes are shown in Figure 1. Three types of oxygen sites are available on rutile (110): singly coordinated terminal oxygen (TO) sites, doubly coordinated bridging oxygen (BO) sites, and in-plane triply coordinated oxygen (IO) sites.[23,24] Because the IO site is inert with respect to adsorption reactions,[23] only TO and BO sites are available to coordinate with As(V).[24−26]

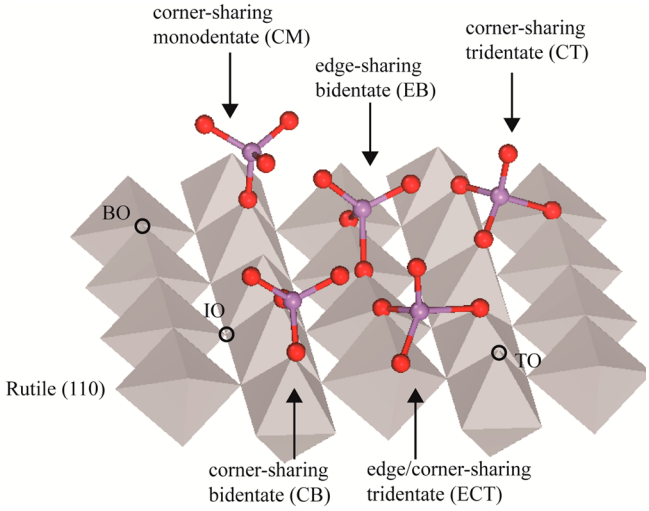

Figure 1. Schematic representations of rutile (110) and As(V) surface complexes. TO, BO, and IO represent singly coordinated terminal oxygen site, doubly coordinated bridging oxygen site, and in-plane triply coordinated oxygen site, respectively.

Five possible As(V) surface complexes were considered in the study (Figure 1). A corner-sharing monodentate (CM) structure exists on TO sites, where the AsO_4 tetrahedra share the summit oxygen atom of the TiO_6 octahedra.[8,9] Two

dx.doi.org/10.1021/jp500097v | J. Phys. Chem. A 2014, 118, 4759−4765

bidentate As(V) surface complexes were considered: a corner-sharing bidentate complex (CB) on TO sites[8,9,27−29] and an edge-sharing bidentate complex (EB) on BO sites.[27,28] Two possible tridentate complexes were also considered: a corner-sharing tridentate (CT) and an edge/corner-sharing tridentate (ECT) configuration. These five surface complexes of mono-, bi-, and tridentate coordination for the As(V)-rutile system were geometrically optimized using DFT+U calculations in the water model. Then, the optimized structures were extracted to fit the GI-XAFS spectra. The structure parameters for the optimized adsorption complexes are shown in the SI.

As K-Edge GI-XAFS Analysis. The As K-edge GI-XAFS spectra are shown in Figure 2a, and the fitting results are summarized in Table 1. The FT peak distances in Figure 2b were not corrected for the phase shift, and thus denoted as $R+\Delta$ to distinguish these distances from the interatomic distances, R, as described in Table 1.

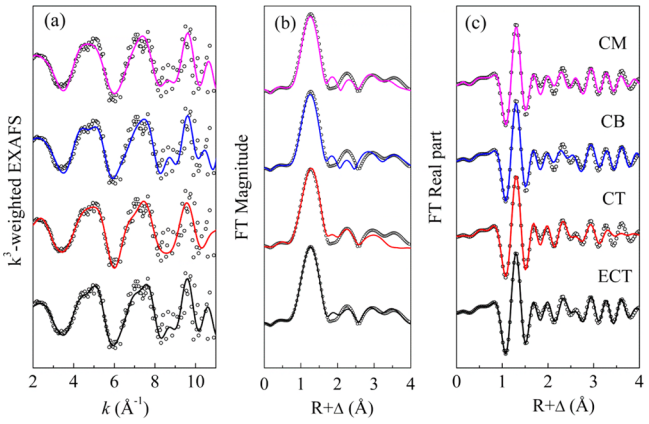

Figure 2. Normalized k^3-weighted observed (dotted line) and model-calculated (solid line) (a) As K-edge XAFS, and (b) the corresponding magnitude of Fourier transform and (c) real part of FT spectra for As(V) adsorption on rutile (110) with CM, CB, CT, and ECT configurations.

Corner-Sharing Monodentate (CM) and Bidentate (CB) Structures. The GI-XAFS fitting results (Table 1) showed that the first As coordination shell consisted of four oxygen atoms at a distance of 1.68−1.70 Å, which is in agreement with EXAFS studies of As(V) adsorption on aluminum, iron, and titanium oxides.[2,8,9] The distinct feature at the region of $R+\Delta \approx 3.0$ Å (Figure 2c) was best fitted with 0.3 Ti neighbors at 3.36 Å for the CM structure, and 1.5 Ti atoms at 3.37 Å for CB. The As−Ti distances obtained with GI-XAFS were slightly longer than our previously reported values (3.27−3.30 Å) in a bidentate binuclear configuration, obtained using powder XAFS analysis.[2,3] This difference in the As−Ti distance may be attributable to the adsorbent, i.e., single crystal rutile (110) in this study and anatase powder in previous reports. The FT spectra also show that there was a strong contribution around $R+\Delta \approx 3.5$ Å, corresponding to a single scattering from an As−O shell at 3.97 Å for the CM adsorption structure, or As−Ti shells at 4.03 Å for the CB adsorption structure. However, there was no Ti or O backscattering able to fit the peak in the FTs at $R+\Delta \approx 2.3$ Å (Figure 2b CM and CB).

To improve the GI-XAFS fitting in the R range 2.8−3.3 Å, a MS path of As−O−O within the AsO_4 tetrahedra was also considered.[8,30] However, our results indicated that the strong feature in the FTs at $R+\Delta \approx 2.3$ Å cannot be fitted using this MS path approach. As detailed in SI Figure S2 and Table S1, this conclusion was further justified using the Hamilton test on the goodness of fit, the R-factor.[31]

Edge-Sharing Bidentate (EB) Structure. The EB adsorption structure, where an adsorbed AsO_4 tetrahedron shares an edge with TiO_6 octahedra, was also considered in our work. Nevertheless, no reasonable GI-XAFS fitting could be achieved using this EB structure, indicating that the EB configuration might not be favorable in this study. This conclusion was further verified by the DFT-calculated adsorption energy in Table 2 and Pauling bond valence principle (vide infra). Consistent with our results, a previous EXAFS study found that Fe(III)-O octahedra would undergo appreciable distortion if As(V) forms an edge-sharing bidentate (EB) adsorption complex on ferrihydrite.[32] In contrast, some researchers argued

Table 1. As K-Edge GI-XAFS Shell-Fit Results and DFT+U Calculated Geometry for As(V)-Rutile (110) Interfacial Structures[a]

structure	shell	CN	R(Å)	σ^2(Å^2)	ΔE(eV)	R-factor	R_c(Å)
corner-sharing monodentate structure (CM)	As−O	4[b]	1.68	0.001	3.5	0.016	1.71
	As−O−O	12[b]	3.00	0.001			
	As−Ti	0.3	3.36	0.002			3.58
	As−O	1.5	3.97	0.002[b]			4.19
corner-sharing bidentate structure (CB)	As−O	4[b]	1.68	0.001	4.3	0.013	1.71
	As−O−O	12[b]	3.05	0.001			
	As−Ti	1.5	3.37	0.0002			3.31
	As−Ti	0.9	4.03	0.0015			4.14
corner-sharing tridentate structure (CT)	As−O	4[b]	1.70	0.001	8.3	0.013	1.72
	As−O−O	12[b]	3.23	0.001			
	As−O	1.1	2.72	0.003			2.71
	As−Ti	4.8	3.36	0.011			3.28
edge/corner- sharing tridentate structure (ECT)	As−O	4[b]	1.70	0.001	6.9	0.0042	1.72
	As−O−O	12[b]	3.22	0.001			
	As−Ti	1.3	2.83	0.004			2.85
	As−Ti	0.4	3.36	0.002			3.42
	As−Ti	1.8	4.05	0.002			4.05

[a]Note. CN is the coordination number. R is the mean half path length. σ^2 is the Debye−Waller factor. ΔE is the Energy-shift parameter. R_c is the DFT+U calculated interatomic distances in the water model. [b]This parameter was fixed.

dx.doi.org/10.1021/jp500097v | J. Phys. Chem. A 2014, 118, 4759−4765

Table 2. Adsorption Energy (eV) of As(V) on Rutile (110) in the Water Model for Different Adsorption Structures

structure	$E_{As+surf}$	E_{surf}	E_{As}	E_{ads}
CM	−81199.500	−79288.538	−1910.239	−0.723
CB	−81199.880	−79288.538	−1910.239	−1.103
CT	−80768.649	−78853.131	−1910.239	−5.279
EB	−80330.148	−78413.727	−1910.239	−6.182
ECT	−80331.625	−78413.727	−1910.239	−7.659

that EB could exist on Fe oxides based on a shorter As−Fe distance at about 2.82 Å.[6,27,28,33]

Tridentate (CT and ECT) Adsorption Structures. For the CT surface complex, the results of the first As−O shell and MS path were similar to that in the CM and CB structures (Table 1). However, the strong feature in the FTs at $R+\Delta \approx 2.3$ Å corresponded to the second As−O shell with 1.1 in-plane O atoms (IO site in Figure 1) at about 2.72 Å. The distinct peak at the region of $R+\Delta \approx 3.0$ Å was best fitted with 4.8 Ti neighbors at 3.36 Å (Table 1). However, no suitable path in the CT complex can result in a reasonable fit to the peak at $R+\Delta \approx 3.5$ Å (Figure 2b CT).

To establish the ECT surface complex, the AsO_4 tetrahedra share an edge with the Ti octahedra, with the third O atom in AsO_4 on the apex of adjacent TiO_6 (Figure 1). The FT spectrum (Figure 2b ECT) exhibited a first As−O shell ($R+\Delta \approx 1.3$ Å, $R = 1.70$ Å) and a second As−Ti shell ($R+\Delta \approx 2.3$ Å, $R = 2.83$ Å). This short As−Ti distance was comparable to that of As−Fe (2.75−2.86 Å) observed in XAFS studies of As(V) adsorption on Fe oxides.[6,27,28,33] The ECT structure resulted in two more As−Ti shells: one at a distance of 3.36 Å with a CN of 0.4, and the other at 4.05 Å with a CN of 1.8.

DFT+U Calculation Results. A comparison of GI-XAFS results with the DFT+U calculated geometry is shown in Table 1. Our DFT-calculated As−Ti distances in CM (3.58 Å) and CB (3.31 Å) structures were in line with a previous DFT study.[11] However, the DFT-calculated As−Ti distances deviated from experimentally measured values (3.36−3.37 Å). For the CT structure, the DFT+U calculations suggested a shorter As−Ti distance of 3.28 Å compared with the experimentally determined value (3.36 Å). The failure of the CM, CB, and CT models to fit the GI-XAFS data implied that the corner-sharing surface configuration may not be favorable in our present study.

For the ECT structure, the DFT+U calculated geometry agreed well with our GI-XAFS results, indicating that this ECT structure should be preferred. In addition, the fact that this configuration had the lowest DFT+U E_{ads} (−7.659 eV) further confirmed this conclusion (Table 2).

Adsorption Energy Comparison. The DFT+U calculations showed that the five As(V) surface configurations were thermodynamically favorable on rutile (110) as evidenced by their negative adsorption energies (E_{ads}, Table 2). The calculated E_{ads} of a surface complex should be appropriately viewed relative to alternative structures, rather than individually by absolute value. ECT resulted in the lowest E_{ads} and most stable configuration. Though EB had the second lowest E_{ads}, it did not lead to a reasonable GI-XAFS fitting. Both the results of GI-XAFS and adsorption energy suggested that the ECT surface complex is the most favorable configuration for As(V) on rutile (110). Achieving a detailed understanding of the ECT electronic configuration motivated our electron density and partial density of states (PDOS) analysis.

The hydration effect is another consideration when modeling a surface complex at the mineral−water interface. Our modeling results showed that E_{ads} is slightly higher in the presence of water molecules than in a vacuum (SI Table S2). This slight increase in E_{ads} could be explained by the fact that surrounding water molecules tend to form a "cage" to trap AsO_4 and inhibit its access to the rutile surface.[17] The comparison of the surface complex geometry in vacuum and the water model shown in SI Table S3 suggested that the optimized surface configuration in the water model is closer to the GI-XAFS fitting results.

Electron Density and PDOS Analysis. The change in electron density of a local surface complex provides additional evidence of the adsorption interaction.[17,18,34] Upon adsorption, a significant repolarization of the electron density occurred around AsO_4 and rutile (110) in the ECT surface complex (Figure 3). Figure 3a shows the electron density difference

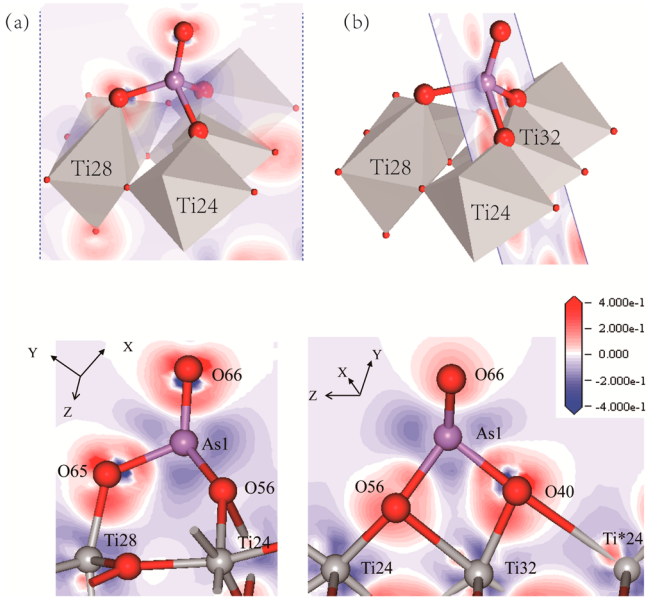

Figure 3. Electron density difference slices for ECT surface complex. The charge accumulation and depletion are represented by red and blue, respectively. Symmetry-paired atoms are denoted by an asterisk.

($\Delta\rho$) slice passing through O and As of AsO_4, and surface Ti ($As_1-O_{65}-Ti_{28}$); this Ti−O bond corresponds to one O atom in AsO_4 on the apex of an adjacent TiO_6. Figure 3b shows that the AsO_4 tetrahedron shares an edge with the TiO_6 octahedra, corresponding to four Ti−O bonds ($Ti_{24}-O_{56}$, $Ti_{32}-O_{56}$, $Ti_{32}-O_{40}$, and $Ti^*_{24}-O_{40}$). Charge accumulation (in red) was observed near the O_{65}, O_{56}, and O_{40} atoms, and charge depletion (in blue) occurred near the Ti_{28}, Ti_{24}, and Ti_{32} atoms in the surface. Analysis of the electron density difference demonstrated that charge transfer occurred between surface Ti atoms and O atoms of AsO_4. Such charge transfer consequently induced the formation of a chemical bond, which was further confirmed with the PDOS analysis.

The overlap of PDOS in Figure 4 indicated that four Ti−O atom pairs have the ability to form bonds ($Ti_{28}-O_{65}$, $Ti_{24}-O_{56}$, $Ti_{32}-O_{56}$, and $Ti_{32}-O_{40}$), which was consistent with the electron density difference results. Figure 5 shows the PDOS of coordinated O and Ti before and after adsorption. By comparing the PDOS of uncoordinated O_{66} with the other three coordinated O atoms (O_{65}, O_{56}, and O_{40}), the energy of

dx.doi.org/10.1021/jp500097v | J. Phys. Chem. A 2014, 118, 4759−4765

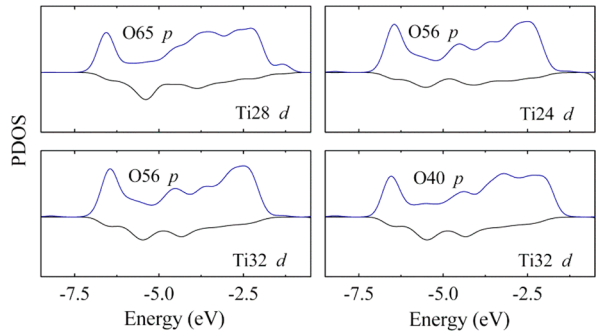

Figure 4. PDOS for ECT surface complex. O_{65}, O_{56}, O_{40}, and Ti_{28}, Ti_{24}, Ti_{32} are highlighted in Figure 3.

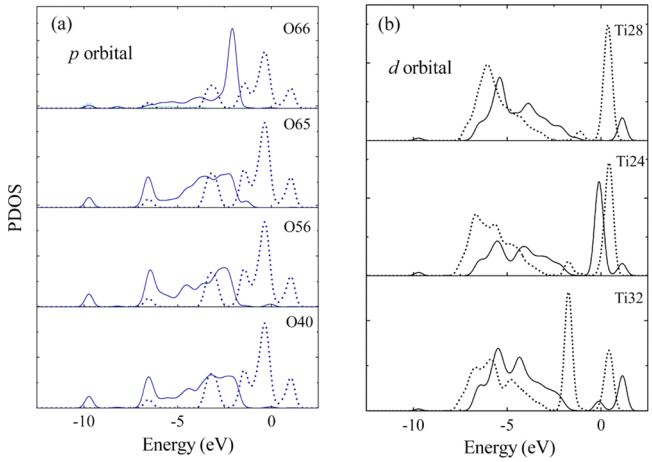

Figure 5. PDOS of O_{66}, O_{65}, O_{56}, O_{40} (a); and Ti_{28}, Ti_{24}, Ti_{32} (b) before (dotted line) and after (solid line) adsorption for ECT surface complex.

coordinated O atoms was lowered, and their p orbital energy was located between −7.5 and −1.3 eV (Figure 5a), in the same energy range as the Ti-d orbitals (Figure 5b). Thus, the major contribution of new Ti−O bonds was due to electron sharing between O-p and Ti-d orbitals.[35]

The $\Delta\rho$ and PDOS results for other surface complexes (EB, CT, CB, and CM) are detailed in the SI. The EB surface complex has results similar to the ECT structure, such that the p orbital energy of coordinated O atoms in the range −4.2 to 2.0 eV was reduced to the range of −7.5 to −1.3 eV to match the Ti-d orbital energy (SI Figure S8). However, the PDOS results of the three corner-sharing surface complexes (CT, CB, and CM) suggested that the coordinated O-p orbital energy was lowered to the range of −6.2 to 0.0 eV to match the Ti-d orbital energy (SI Figure S9−11). The results indicated that the formation mechanism of corner-sharing and edge-sharing surface complexes is different. In corner-sharing surface complexes, the Ti−O bonds newly formed upon adsorption can be attributed to the O-p and Ti-d orbitals with high energy (−6.2 to 0.0 eV), indicating that these bonds are less stable than those with low hybrid orbital energy (−7.5 to −1.3 eV) in edge-sharing complexes. In agreement with our E_{ads} analysis in Table 2, $\Delta\rho$ and PDOS results confirmed our conclusion that the edge-sharing surface configuration is more favorable. The structural discrepancy between EB and ECT is further highlighted by the following analysis using the Pauling bond valence principle.

Pauling Bond Valence Principle for EB and ECT Configuration. The Pauling bond valence, S, is determined by Z/CN, where Z is the charge of the central ion, and CN is the coordination number.[36] To take into account the bond length, S is formulated as[37] $S = S_0(R/R_0)^{-n}$, where S_0, R_0, and n are characteristics of each cation−anion pair. For As(V)−O pairs, $R_0 = 1.746$ and $n = 6.050$.[37] The DFT-calculated Mulliken charge (Z) and bond length (R) are shown in Table 3. For the ECT surface complex, the CN for O_{66}, O_{65}, O_{56}, and O_{40} was 1, 2, 3, and 3, respectively (Figure 3). For the EB surface complex, the CN for O_{66}, O_{65}, O_{56}, and O_{40} was 1, 1, 3, and 3, respectively (SI Figure S3a). Then, the corresponding As−O bond strength was calculated, and the results are shown in Table 3. For the ECT surface complex, the total As−O bond strength was −2.193, which is comparable to the Mulliken charge of As (1.96). For the EB structure, the total As−O bond strength (−3.052) deviated from the charge of As (1.99). The As−O bond in the ECT structure satisfied the Pauling bond valence principle that the total strength of the valence bonds reaching an anion from all neighboring cations is equal to the charge of the anion. The results suggest that the ECT structure should be more stable than EB, which is in line with our adsorption energy calculation and GI-XAFS results.

4. CONCLUSIONS

The local coordination environment of As(V) on the rutile (110) surface was determined using GI-XAFS and DFT+U calculations. The results offer clear evidence that As(V) bound in an inner-sphere fashion with the edge/corner-sharing tridentate (ECT) complex is the most favorable adsorption configuration. The existence of this ECT complex on the metal oxide/aqueous interface improves our understanding of possible As(V) surface configurations, which play an important role in the fate and transport of As(V) in the environment. In addition, the results show that spectroscopic data alone is not sufficient to determine the nature of adsorption complexes on the molecular scale. Molecular modeling such as DFT calculations facilitates the accurate interpretation of the results.

Table 3. DFT+U Calculated Mulliken Charge and Bond Length of AsO_4 for ECT and EB Surface Complexes

	Mulliken charge			bond length (Å)		bond strength	
atoms	ECT	EB	band type	ECT	EB	ECT	EB
As1	1.96	1.99					
O66	−0.85	−0.92	O66−As1	1.635	1.652	−1.267	−1.288
O65	−0.77	−0.91	O65−As1	1.736	1.658	−0.398	−1.243
O56	−0.85	−0.86	O56−As1	1.748	1.776	−0.282	−0.259
O40	−0.82	−0.86	O40−As1	1.776	1.773	−0.247	−0.261

dx.doi.org/10.1021/jp500097v | J. Phys. Chem. A 2014, 118, 4759−4765

■ ASSOCIATED CONTENT

Supporting Information

Description of *R*-factor test; tables showing hydration effect, optimized adsorption configurations; figures showing experimental setup, electron density difference, and PDOS analysis. This material is available free of charge via the Internet at http://pubs.acs.org.

■ AUTHOR INFORMATION

Corresponding Author

*Tel: +86 10 6284 9523. Fax: +86 10 6284 9523. E-mail: cyjing@rcees.ac.cn.

Notes

The authors declare no competing financial interest.

■ ACKNOWLEDGMENTS

We acknowledge the financial support of the National Basic Research Program of China (2014CB114402), the Strategic Priority Research Program of the Chinese Academy of Sciences (XDB14020201), the National Natural Science Foundation of China (41373123 and 21321004), and RCEES (YSW2013A01).

■ REFERENCES

(1) Chen, X.; Mao, S. S. Titanium Dioxide Nanomaterials: Synthesis, Properties, Modifications, and Applications. *Chem. Rev.* **2007**, *107*, 2891−2959.

(2) Pena, M.; Meng, X.; Korfiatis, G. P.; Jing, C. Adsorption Mechanism of Arsenic on Nanocrystalline Titanium Dioxide. *Environ. Sci. Technol.* **2006**, *40*, 1257−1262.

(3) Jing, C.; Liu, S.; Patel, M.; Meng, X. Arsenic Leachability in Water Treatment Adsorbents. *Environ. Sci. Technol.* **2005**, *39*, 5481−5487.

(4) Trainor, T. P.; Fitts, J. P.; Templeton, A. S.; Grolimund, D.; Brown, G. E. Grazing-Incidence XAFS Study of Aqueous Zn(II) Sorption on α-Al_2O_3 Single Crystals. *J. Colloid Interface Sci.* **2001**, *244*, 239−244.

(5) Bargar, J. R.; Trainor, T. P.; Fitts, J. P.; Chambers, S. A.; Brown, G. E. In Situ Grazing-Incidence Extended X-ray Absorption Fine Structure Study of Pb(II) Chemisorption on Hematite (0001) and (1−102) Surfaces. *Langmuir* **2004**, *20*, 1667−1673.

(6) Waychunas, G.; Trainor, T.; Eng, P.; Catalano, J.; Brown, G.; Davis, J.; Rogers, J.; Bargar, J. Surface Complexation Studied via Combined Grazing-Incidence EXAFS and Surface Diffraction: Arsenate on Hematite (0001) and (10−12). *Anal. Bioanal. Chem.* **2005**, *383*, 12−27.

(7) Waychunas, G. A. Grazing-Incidence X-ray Absorption and Emission Spectroscopy. *Applications of Synchrotron Radiation in Low-Temperature Geochemistry and Environmental Sciences* **2002**, *49*, 267−315.

(8) Sherman, D. M.; Randall, S. R. Surface Complexation of Arsenic(V) to Iron(III) (Hydr)oxides: Structural Mechanism from ab initio Molecular Geometries and EXAFS Spectroscopy. *Geochim. Cosmochim. Acta* **2003**, *67*, 4223−4230.

(9) Ladeira, A. C. Q.; Ciminelli, V. S. T.; Duarte, H. A.; Alves, M. C. M.; Ramos, A. Y. Mechanism of Anion Retention from EXAFS and Density Functional Calculations: Arsenic (V) Adsorbed on Gibbsite. *Geochim. Cosmochim. Acta* **2001**, *65*, 1211−1217.

(10) Blanchard, M.; Morin, G.; Lazzeri, M.; Balan, E.; Dabo, I. First-Principles Simulation of Arsenate Adsorption on the (1−12) Surface of Hematite. *Geochim. Cosmochim. Acta* **2012**, *86*, 182−195.

(11) He, G.; Pan, G.; Zhang, M. Studies on the Reaction Pathway of Arsenate Adsorption at Water−TiO_2 Interfaces using Density Functional Theory. *J. Colloid Interface Sci.* **2011**, *364*, 476−481.

(12) He, G.; Pan, G.; Zhang, M.; Wu, Z. Quantitative XANES Studies on Metastable Equilibrium Adsorption of Arsenate on TiO_2 Surfaces. *J. Phys. Chem. C* **2009**, *113*, 17076−17081.

(13) Ravel, B.; Newville, M. ATHENA, ARTEMIS, HEPHAESTUS: Data Analysis for X-ray Absorption Spectroscopy using IFEFFIT. *J. Synchrotron Radiat.* **2005**, *12*, 537−541.

(14) Loring, J. S.; Sandström, M. H.; Norén, K.; Persson, P. Rethinking Arsenate Coordination at the Surface of Goethite. *Chem.—Eur. J.* **2009**, *15*, 5063−5072.

(15) Clark, S. J.; Segall, M. D.; Pickard, C. J.; Hasnip, P. J.; Probert, M. I. J.; Refson, K.; Payne, M. C. First Principles Methods using CASTEP. *Z. Kristallogr.* **2005**, *220*, 567−570.

(16) San-Miguel, M. A.; Amorim, E. P. M.; da Silva, E. Z. Adsorption of Pd, Pt, Cu, Ag, and Au Monomers on NiAl(110) Surface: A Comparative Study from DFT Calculations. *J. Phys. Chem. A* **2013**, DOI: /10.1021/jp405877k.

(17) Guo, Y.; Lu, X.; Zhang, H.; Weng, J.; Watari, F.; Leng, Y. DFT Study of the Adsorption of Aspartic Acid on Pure, N-Doped, and Ca-Doped Rutile (110) Surfaces. *J. Phys. Chem. C* **2011**, *115*, 18572−18581.

(18) Ye, C.; Hu, S.; Yan, W.; Duan, J.; Jing, C. Insights into Propranolol Adsorption on TiO_2: Spectroscopic and Molecular Modeling Study. *J. Phys. Chem. C* **2013**, *117*, 5785−5791.

(19) Hu, Z.; Metiu, H. Choice of U for DFT+U Calculations for Titanium Oxides. *J. Phys. Chem. C* **2011**, *115*, 5841−5845.

(20) Chrétien, S.; Metiu, H. Electronic Structure of Partially Reduced Rutile TiO_2(110) Surface: Where Are the Unpaired Electrons Located? *J. Phys. Chem. C* **2011**, *115*, 4696−4705.

(21) Tilocca, A.; Selloni, A. DFT-GGA and DFT+ U Simulations of Thin Water Layers on Reduced TiO_2 Anatase. *J. Phys. Chem. C* **2012**, *116*, 9114−9121.

(22) Kumar, N.; Kent, P. R. C.; Wesolowski, D. J.; Kubicki, J. D. Modeling Water Adsorption on Rutile (110) Using van der Waals Density Functional and DFT+U Methods. *J. Phys. Chem. C* **2013**, *117*, 23638−23644.

(23) Bourikas, K.; Hiemstra, T.; Van Riemsdijk, W. H. Ion Pair Formation and Primary Charging Behavior of Titanium Oxide (Anatase and Rutile). *Langmuir* **2001**, *17*, 749−756.

(24) Vandenborre, J.; Drot, R.; Simoni, E. Interaction Mechanisms between Uranium(VI) and Rutile Titanium Dioxide: From Single Crystal to Powder. *Inorg. Chem.* **2007**, *46*, 1291−1296.

(25) Zhang, Z.; Fenter, P.; Cheng, L.; Sturchio, N. C.; Bedzyk, M. J.; Předota, M.; Bandura, A.; Kubicki, J. D.; Lvov, S. N.; Cummings, P. T.; et al. Ion Adsorption at the Rutile−Water Interface: Linking Molecular and Macroscopic Properties. *Langmuir* **2004**, *20*, 4954−4969.

(26) Towle, S. N.; Brown, G. E.; Parks, G. A. Sorption of Co(II) on Metal Oxide Surfaces I. Identification of Specific Binding Sites of Co(II) on (110) and (001) Surfaces of TiO_2 (Rutile) by Grazing-Incidence XAFS Spectroscopy. *J. Colloid Interface Sci.* **1999**, *217*, 299−311.

(27) Manceau, A. The Mechanism of Anion Adsorption on Iron Oxides: Evidence for the Bonding of Arsenate Tetrahedra on Free $Fe(O, OH)_6$ Edges. *Geochim. Cosmochim. Acta* **1995**, *59*, 3647−3653.

(28) Fendorf, S.; Eick, M. J.; Grossl, P.; Sparks, D. L. Arsenate and Chromate Retention Mechanisms on Goethite. 1. Surface Structure. *Environ. Sci. Technol.* **1997**, *31*, 315−320.

(29) Waychunas, G. A.; Rea, B. A.; Fuller, C. C.; Davis, J. A. Surface Chemistry of Ferrihydrite: Part 1. EXAFS Studies of the Geometry of Coprecipitated and Adsorbed Arsenate. *Geochim. Cosmochim. Acta* **1993**, *57*, 2251−2269.

(30) Gurman, S. J.; Binsted, N.; Ross, I. A Rapid, Exact, Curved-Wave Theory for EXAFS Calculations. II. The Multiple-Scattering Contributions. *J. Phys. C: Solid State Phys.* **1986**, *19*, 1845−1861.

(31) Hamilton, W. C. Significance Tests on the Crystallographic R Factor. *Acta Crystallogr.* **1965**, *18*, 502−510.

(32) Waychunas, G. A.; Davis, J. A.; Fuller, C. C. Geometry of Sorbed Arsenate on Ferrihydrite and Crystalline FeOOH: Re-evaluation of EXAFS Results and Topological Factors in Predicting Sorbate Geometry, and Evidence for Monodentate Complexes. *Geochim. Cosmochim. Acta* **1995**, *59*, 3655−3661.

(33) Arai, Y.; Sparks, D. L.; Davis, J. A. Effects of Dissolved Carbonate on Arsenate Adsorption and Surface Speciation at the Hematite−Water Interface. *Environ. Sci. Technol.* **2003**, *38*, 817−824.
(34) Zhang, P.; Zhang, D.; Huang, L.; Wei, Q.; Lin, M.; Ren, X. First-Principles Study on the Electronic Structure of a $LiFePO_4$ (010) Surface Adsorbed with Carbon. *J. Alloys Compd.* **2012**, *540*, 121−126.
(35) Li, Y.; Liu, Z. Particle Size, Shape and Activity for Photocatalysis on Titania Anatase Nanoparticles in Aqueous Surroundings. *J. Am. Chem. Soc.* **2011**, *133*, 15743−15752.
(36) Machesky, M. L.; Wesolowski, D. J.; Palmer, D. A.; Ridley, M. K. On the Temperature Dependence of Intrinsic Surface Protonation Equilibrium Constants: An Extension of the Revised MUSIC Model. *J. Colloid Interface Sci.* **2001**, *239*, 314−327.
(37) Brown, I. D.; Shannon, R. D. Empirical Bond-Strength-Bond-Length Curves for Oxides. *Acta Crystallogr., Sect. A* **1973**, *29*, 266−282.